

Direct Band-to-Band Tunneling in Reverse Biased MoS₂ Nanoribbon p-n Junctions

Ram Krishna Ghosh and Santanu Mahapatra, *Senior Member, IEEE*

Abstract—We investigate the direct band-to-band tunneling (BTBT) in a reverse biased molybdenum disulfide (MoS₂) nanoribbon p-n junction by analyzing the complex band structure obtained from semiempirical extended Hückel method under relaxed and strained conditions. It is demonstrated that the direct BTBT is improbable in relaxed monolayer nanoribbon; however, with the application of certain uniaxial tensile strain, the material becomes favorable for it. On the other hand, the relaxed bilayer nanoribbon is suitable for direct BTBT but becomes unfavorable when the applied uniaxial tensile or compressive strain goes beyond a certain limit. Considering the Wentzel–Kramers–Brillouin approximation, we evaluate the tunneling probability to estimate the tunneling current for a small applied reverse bias. Reasonably high tunneling current in the MoS₂ nanoribbons shows that it can take advantage over graphene nanoribbon in future tunnel field-effect transistor applications.

Index Terms—Bandgap, band-to-band tunneling (BTBT), complex band structure, nanoribbon, strain.

I. INTRODUCTION

THE TUNNEL field-effect transistor (TFET) has emerged as a strong candidate for next-generation low-standby-power (LSTP) applications due to its sub-60-mV/dec subthreshold slope (SS) [1]–[4]. However, the large indirect energy bandgap (~ 1.12 eV) of silicon results in high value of “least action integral” [5], and thus, it is difficult to achieve low SS and high ON current from the conventional silicon TFETs. As a result, alternative channel materials for TFET are being investigated, which might have lower value of “least action integral” [3], [6] and do not require phonon assistance that reduces the transmission rate in the tunneling process. After the discovery of graphene, atomically thin layered materials have been found to have great significance as alternate MOSFET channel materials due to their excellent electrostatic integrity, planar structure, and mechanical flexibility. Recent studies show that the graphene nanoribbon (GNR) TFETs, having sub-10-nm channel width, can achieve much higher I_{ON} – I_{OFF} ratio and much smaller SS than the limit of MOSFET [7]. However, it has been also observed that the bandgap of GNR decreases as its width increases and approaches to zero when it goes beyond 5 nm [8], [9]. Thus, the practical application of GNR as TFET

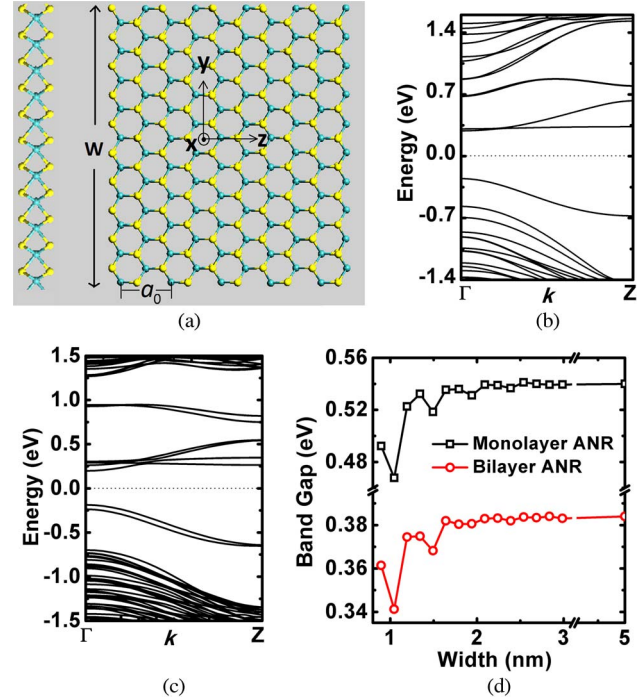


Fig. 1. (a) Atomistic structure of relaxed MoS₂ ANR (monolayer). The transport direction is along the z -direction. Color code: Green = Mo and yellow = S. Energy band structure of (b) monolayer MoS₂ ANR and (c) bilayer MoS₂ ANR having 5-nm width using ATK builder which uses an extended Hückel approach. (d) Plot of the energy bandgaps in relaxed monolayer and bilayer MoS₂ ANRs as a function of ribbon width.

channel material is questionable as the very small bandgap might result in an increase of OFF-state leakage, which is a major concern for LSTP applications.

As an alternative to graphene, recently, layered transition-metal dichalcogenide materials, particularly MoS₂, has attracted much attention for its application in nanoscale MOSFET channel material [10]–[12]. Monolayer MoS₂ has a direct band (~ 1.8 eV), whereas with the increase of layers, the bandgap becomes indirect and reduces to 1.23 eV in its bulk crystal form [13], [14]. The layered MoS₂ nanoribbons can be constructed then by cutting from these MoS₂ layers with the desired width (W) and edge priority. It is demonstrated that the MoS₂ nanoribbons having an armchair edge (MoS₂ ANRs) [Fig. 1(a)] are semiconducting and nonmagnetic in nature, whereas the zigzag edges (MoS₂ ZNRs) exhibit metallic and magnetic nature [15]–[17]. It is also found that the bandgap (E_g) of intrinsic MoS₂ ANR is a direct one and much smaller than the MoS₂ sheet due to the presence of strongly localized quasi-1-D states at the edges [Fig. 1(b) and (c)]. It has been seen that this

Manuscript received September 26, 2012; accepted October 23, 2012. Date of publication November 19, 2012; date of current version December 19, 2012. The review of this paper was arranged by Editor R. K. Lake.

The authors are with the Nano-Scale Device Research Laboratory, Department of Electronic Systems Engineering, Indian Institute of Science, Bangalore 560012, India (e-mail: ramki.phys@gmail.com; santanu@cedt.iisc.ernet.in).

Color versions of one or more of the figures in this paper are available online at <http://ieeexplore.ieee.org>.

Digital Object Identifier 10.1109/TED.2012.2226729

bandgap starts oscillating for very thin ribbons (within 3-nm width) and it converges to 0.54 eV when W increases to a larger dimension [Fig. 1(d)]. In multilayer nanoribbons, even a weaker interlayer interaction plays a crucial role, and the saturated direct bandgap value decreases monotonically with the increasing number of layers, as can be seen in Fig. 1(d)[17]. Therefore, to reduce the effective tunneling barrier height by replacing the Si with a smaller bandgap material, MoS_2 ANR can be more useful as an alternative TFET material than MoS_2 layered sheets.

In this work, we explore the band-to-band tunneling (BTBT) in monolayer and bilayer MoS_2 nanoribbon reverse biased p-n junctions by considering the complex dispersion relationship within the bandgap region. These complex band structure calculations have been evaluated by using the Atomistix ToolKit (ATK) which uses a semiempirical approach by taking the extended Hückel method [18]. Furthermore, the elastic uniaxial strain effect on this BTBT has also been investigated. The present work can be put forward to analyze the performance of MoS_2 TFET by taking into account the gate electric field appropriately.

II. THEORETICAL APPROACH, RESULTS AND DISCUSSIONS

During the BTBT process, when a carrier tunnels through a bandgap region, physically, it transits in an evanescent mode, and its wave vector becomes imaginary within this forbidden gap. Recently, this complex band theory has been successfully applied in the modeling of tunneling devices [19], [20]. In this work, the complex band structure calculations of geometrically optimized MoS_2 ANRs have been carried out by using the ATK simulator. Our computations are based on the semiempirical extended Hückel method instead of the usual density-functional theory (DFT) method [21]. This has been used due to two main reasons: First, it is well known that the DFT calculation does not provide a good estimation of the energy bandgap, and second, the extended Hückel approach is computationally more efficient and provides good convergence. The Hückel basis set used for the computations included Cerda molybdenum [22] and Hoffman sulfur having vacuum energy levels of -5.1942 and 0 eV, respectively, with a Wolfsberg weighting scheme. The tolerance parameter was 10^{-5} with maximum steps of 200, and a Pulay mixer algorithm [23] was used as the iteration control parameter. In addition, the k -point sampling of $1 \times 1 \times 51$ grid was used with a mesh cutoff energy of 10 Hartree. In all computations, we have strictly maintained the same aforementioned control parameters. The spin-polarized calculations along with the spin-unpolarized ones are also carried out on both unstrained and geometrically optimized MoS_2 ANRs and MoS_2 ZNRs to authenticate for a good agreement with the previous theoretical investigations for real band structures [15]–[17].

Recently, strain engineering has become a convenient procedure to modulate the transport properties of a material and has successfully been employed in the semiconductor industry to improve the carrier mobility in the devices [24], [25]. The strain has a great influence on the electronic band structure properties of materials, although it is rare to achieve large elastic strain for bulk materials because of the fracture issues; on the other

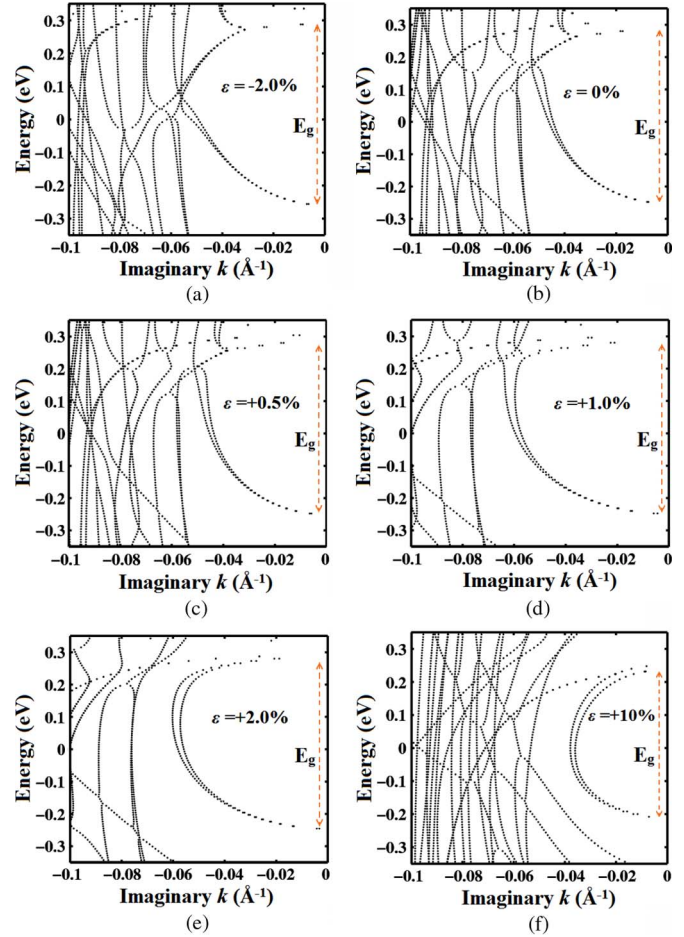


Fig. 2. Complex bands within the forbidden gap (E_g) of 5-nm-wide monolayer MoS_2 ANRs under different elastic uniaxial strains (ϵ). “+” and “-” represent the tensile and compressive strains, respectively.

hand, in layered systems like graphene, high strain can also be achievable, as demonstrated in experiments [26], [27]. In order to explore the elastic strain effect in our study, the strain is applied on the optimized structures of MoS_2 ANRs along the axial z -direction while the other two directions are allowed to be relaxed at that strain. This uniaxial strain is given by scaling the lattice constant of the MoS_2 ANRs by an amount $\epsilon = a - a_0/a_0$, where a_0 and a are the lattice constants for the unit cell of the unstrained MoS_2 ANR and strained MoS_2 ANR, respectively. It should be noted that, due to the fracture and plasticity issues, we can extend the applied strain up to $\epsilon = \pm 11\%$ for the monolayers, while for bilayers, it is up to $\pm 9\%$ achievable, where \pm represents the uniaxial tensile and compressive strain, respectively. The band structure calculation shows that, within these applied strains, the MoS_2 ANRs remain always semiconducting and nonmagnetic in nature.

It should be noted that the interband tunneling probability (T_{BTBT}) depends on the minimum area that is enclosed by the complex band which connects the valence band edge to the conduction band edge [19], [20], [28], [29]. Figs. 2 and 3 show the complex bands within the bandgap regions of 5-nm-width monolayer and bilayer MoS_2 ANRs, respectively, for different strain conditions. For the clarity of the band structures, only few bands are presented here. It should be noted that, in the

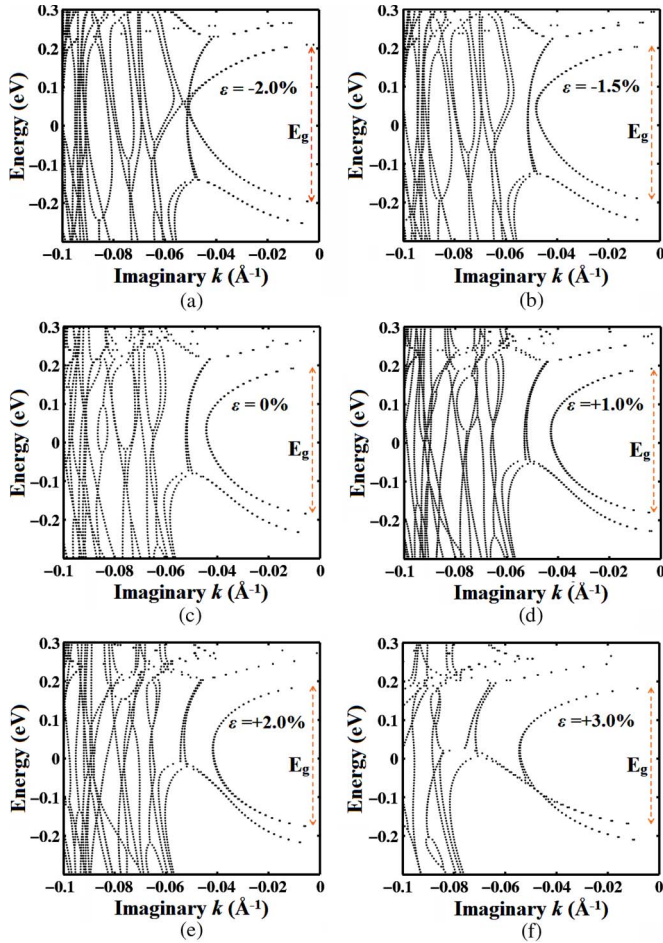


Fig. 3. Complex bands within the forbidden gap (E_g) of 5-nm-wide bilayer MoS_2 ANRs under different elastic uniaxial strains (ε). “+” and “-” represent the tensile and compressive strains, respectively.

case of direct bandgap semiconductors, when the complex band that starts from the top of the valence band “wraps” itself to the bottom of the conduction band, constituting one continuous band, then only the direct BTBT will take place. On the other hand, when the band that starts from the valence band edge does not end up at the conduction band edge but rather “crosses” with the band starting from the conduction band edge, then in the tunneling process, the electron starts to travel along this holelike path and then flips over to the electron-like path after the transition point. This type of feature in the complex band structure requires the inclusion of phonon exchange to ensure the momentum conservation [19]. Thus, this phonon assistance reduces the transmission rate (and, hence, the TFET performance) quite significantly [19], [30]. It is also observed that, in the case of small-bandgap materials, if the energy difference between the direct and indirect bandgaps is quite small, then the transmission probability for direct bandgap transitions dominates over the probability for indirect bandgap transitions [29], [31]. However, since MoS_2 ANRs have a relatively lesser direct bandgap, BTBT probability is reasonably higher than the conventional semiconducting channel materials.

From Fig. 2(b), one can find that, in the case of relaxed monolayer MoS_2 ANR, the complex band that starts from the top of the valence band crosses with the band starting from the con-

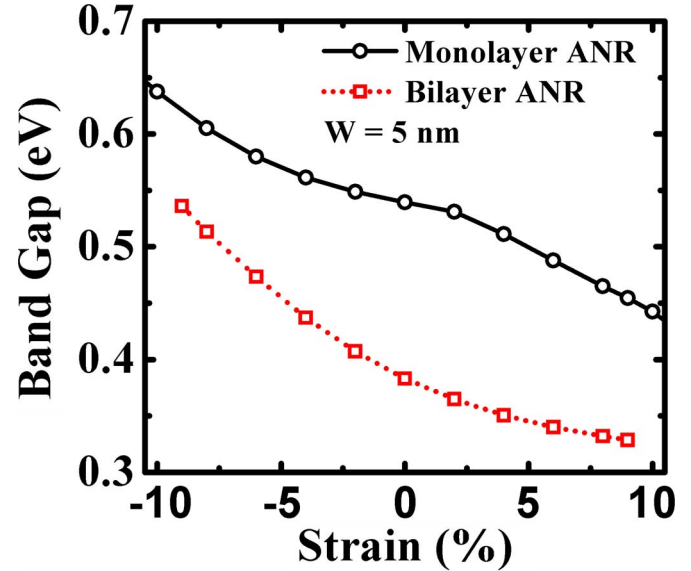


Fig. 4. Variation of energy bandgaps of monolayer and bilayer MoS_2 ANRs under uniaxial tensile and compressive strains.

duction band edge. Hence, in this situation, the transition will need a phonon-assisting process. Now, if we provide a tensile uniaxial strain along the transport direction, then it appears from Fig. 2(c)–(f) that, at +1% strain, the complex band from the top of the valence band starts wrapping itself rather than crossing, and when the tensile strain increases above +1%, the band becomes continuous and indicates that the tunneling becomes direct. However, in the compressive strain region, the bands always cross each other [Fig. 2(a)], and therefore, phonon always be needed in the tunneling process. This scenario changes when we move to bilayer MoS_2 ANRs. Fig. 3(c) shows that, in the relaxed condition, the complex band is characterized by a continuous band that connects the highest valence subband to the lowest conduction subband. However, under the strained conditions, when the strain reaches +3% (tensile case) or -2% (compressive case), then the imaginary bands mix with themselves, and the tunneling no longer remains direct [Fig. 3(d)–(f) and Fig. 3(a) and (b)]. Therefore, the strain has great importance in the direct or phonon-assisted tunneling in the cases of both monolayer and bilayer MoS_2 ANRs. It also appears in Fig. 4 that the bandgaps of both monolayer and bilayer MoS_2 ANRs change significantly with the increase in the strain. For monolayer, the bandgap at first decreases slowly up to +2% strain, and then, when we increase the tensile strain further, the bandgap decreases more rapidly. In the compressive zone, the bandgap increases with a faster rate after the -2% strain in a similar fashion. However, in the case of bilayer, the bandgap decreases monotonically when we move from high compressive region to high tensile region. Therefore, for both monolayer and bilayer MoS_2 ANRs, the corresponding tunneling barrier height also decreases with the application of tensile strain. Hence, we can say that such strain application on MoS_2 ANRs will be an encouraging technique to increase the BTBT current in TFET applications.

Now, using the Wentzel–Kramers–Brillouin approximation, the direct tunneling probability (i.e., without phonon assistance)

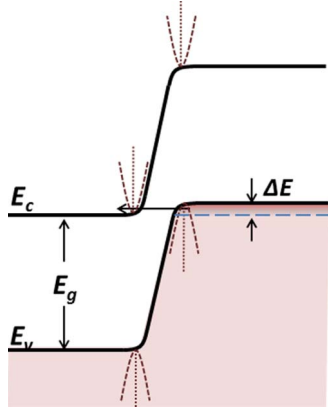


Fig. 5. Schematic band diagram of BTBT in a reverse biased p⁺-n⁺ MoS₂-ANR junctions.

for the BTBT process can be approximated as [30], [32]

$$T_{\text{BTBT}} = \exp \left\{ -\frac{2}{e\xi} \int_0^{E_g} k(E) dE \right\} \equiv \exp \left\{ -\frac{\xi_I}{\xi} \right\} \quad (1)$$

where e is the electronic charge, ξ is the uniform electric field, $E = 0$ is the valence band edge, $E = E_g$ is the conduction band edge, $k(E)$ is the magnitude of the imaginary wave vector with “least action for tunneling” within the forbidden gap, and $\xi_I = 2/e(\int_0^{E_g} k(E)dE)$ is basically the “least action integral” which is an intrinsic property of the ANR. As a result, in any applied electric field, controlled by a third terminal (the gate) in TFET applications, T_{BTBT} can be figured out instantly when it is enumerated. The presence of relatively low bandgap in bilayer MoS₂ ANR shows that the value of ξ_I is quite less than the monolayer, and therefore, the tunneling probability becomes reasonably higher than the monolayer.

Now, we calculate the direct BTBT current (I_{BTBT}) in field-induced p⁺-n⁺ MoS₂-ANR junctions. Here, we consider that, in an electrostatically well-designed device, the Fermi level is at the conduction band edge (E_c) in the n-side and at the valence band edge (E_v) on the p-side at thermal equilibrium (e.g., backward diode). Under this condition, a forward bias cannot lead to current flow, and when a small reverse bias V is applied, then it opens an energy window ΔE over which the current flows, as shown in Fig. 5. We also consider that, when the applied voltage is much smaller than the bandgap, the resulting field due to the voltage is a small fraction of the built-in field at the junction of the MoS₂ ANR whose length is much larger than the width (at least ten times so that the longitudinal momentum of carriers in the ribbon is quasi-continuous). In that approximation, we can neglect the extra field which is justified and makes the actual design of devices conceptually simpler. Under these circumstances, the tunneling current can be then written in the form [33]

$$I_{\text{BTBT}} = \frac{g_s g_v e}{h} \int_0^{\Delta E} T_{\text{BTBT}} \{f_v(E) - f_c(E)\} dE \quad (2)$$

in which h is Planck’s constant; g_s and g_v are the spin and valley degeneracies, respectively, and $f_v(E) = (1/(1 + \exp(E -$

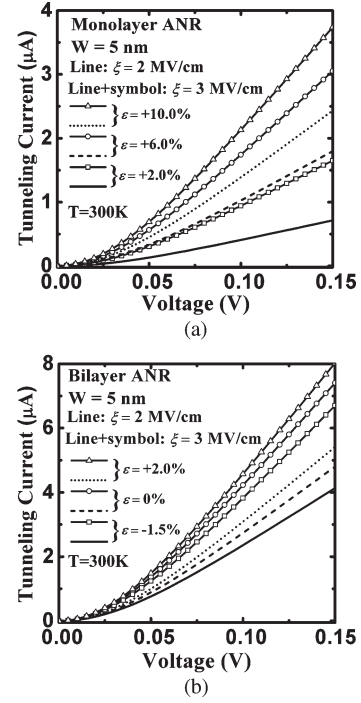


Fig. 6. Tunneling current variation with bias voltages in (a) monolayer MoS₂-ANR and (b) bilayer MoS₂-ANR p⁺-n⁺ junctions for various strains and electric fields at room temperature.

$\Delta E/k_B T$)) and $f_c(E) = (1/(1 + \exp(E/k_B T)))$ are the Fermi functions of the valence and conduction band states from and to which the tunneling occurs, respectively, where k_B is the Boltzmann constant and T is the temperature. Then, the integral in (2) leads to the form

$$I_{\text{BTBT}} = \frac{g_s g_v e}{h} k_B T \ln \left\{ \frac{1}{2} \left(1 + \cosh \frac{\Delta E}{k_B T} \right) \right\} T_{\text{BTBT}}. \quad (3)$$

Fig. 6 shows the variation of the direct BTBT current as a function of bias voltage for monolayer and bilayer MoS₂ ANRs. It appears that, with the increase of the electric field, the tunneling current increases very significantly in both monolayer and bilayer MoS₂ ANRs. However, in the case of bilayer MoS₂ ANR, the current is much higher for a particular electric field due to the higher value of T_{BTBT} and twofold valley degeneracy like bilayer GNR [34]. Fig. 6 also shows the variation of tunneling current in MoS₂ ANR p-n junctions for different strain conditions. It is clear that, in a particular electric field, T_{BTBT} increases significantly as ξ_I decreases with the increase of tensile strain, and hence, the corresponding current also increases. It is observed that, due to the +10% uniaxial strain, we get almost double current than what we achieve in +2% monolayer MoS₂ ANR p-n junctions. Therefore, under tensile strain condition, the I_{BTBT} will increase well for a given external electric field, a trait beneficial for TFET application. Therefore, it clearly indicates that higher BTBT current can be expected for a small reverse bias voltage in MoS₂ ANR p-n junctions.

It also appears that, with the increase of temperature from 300 K to 450 K, the bandgaps of monolayer and bilayer MoS₂ ANRs decrease to only 8.3 and 3.7 meV, respectively, and the nature of complex band structures of both monolayer and

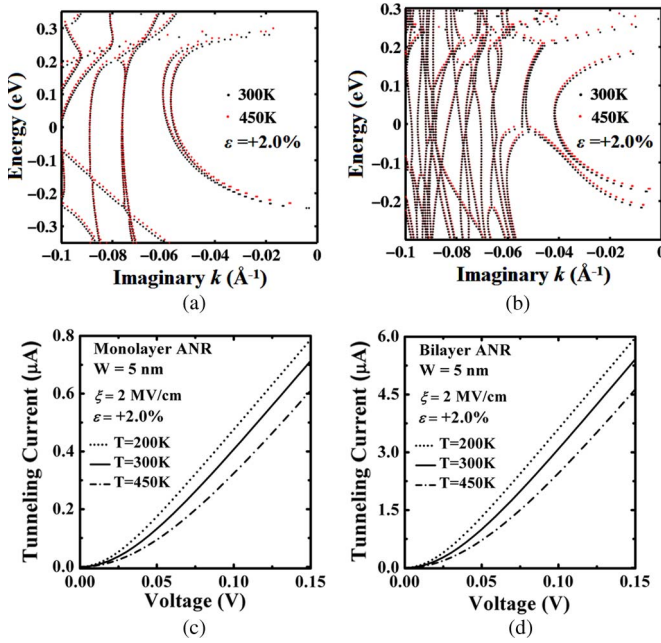


Fig. 7. Complex bands within the forbidden gaps (E_g) of 5-nm-wide +2% strained (a) monolayer and (b) bilayer MoS₂ ANRs at various temperatures. Tunneling current at $\xi = 2$ MV/cm in (c) monolayer and (d) bilayer MoS₂ ANRs at various temperatures.

bilayer MoS₂ ANRs remains almost the same [Fig. 7(a) and (b)]. Due to these negligible changes in bandgaps, Fig. 7(a) and (b) shows that ξ_I remains identical (and so as T_{BTBT} for a particular ξ and ϵ) for both monolayer and bilayer MoS₂ ANRs. Thus, for identical T_{BTBT} , from (3), it could be conceived that, with the decrease of temperature, the tunneling current will increase [Fig. 7(c) and (d)].

Finally, we wish to state that, keeping the computational cost in mind, we have presented here the properties of 5-nm-wide monolayer and bilayer nanoribbons. The results and the methodologies as carried out in this work can be tuned further by modifying the nanoribbon dispersion relation by inclusion of the spin orbit interaction and band coupling that certainly increase the accuracy of our results, although the qualitative features of the complex band structure both in relaxed and strained cases would not change.

III. CONCLUSION

Studying the complex band structure carefully, we have demonstrated that, in relaxed monolayer MoS₂ ANRs, the bands cross each other in the bandgap region, which indicates that the phonon assistance should require for BTBT. However, with the application of tensile strain ($\epsilon \geq +2\%$), the complex band that starts from the top of the valence band wraps itself to the bottom of the conduction band and makes the tunneling as a direct one. However, in the case of bilayer MoS₂ ANRs, the direct tunneling is possible within $-2\% < \epsilon < +3\%$ strain range. Using this, we have investigated the direct tunneling current in the p-n junctions for a small applied reverse bias. We have found that relatively higher tunneling current can be achievable in MoS₂ nanoribbons, and hence, this may become a potential channel material for future TFET applications.

REFERENCES

- [1] J. Appenzeller, Y. M. Lin, J. Knoch, and P. Avouris, "Band-to-band tunneling in carbon nanotube field-effect transistors," *Phys. Rev. Lett.*, vol. 93, no. 19, pp. 196805-1-196805-4, Nov. 2004.
- [2] J. Appenzeller, Y. Lin, J. Knoch, Z. Chen, and P. Avouris, "Comparing carbon nanotube transistors—The ideal choice: A novel tunneling device design," *IEEE Trans. Electron Devices*, vol. 52, no. 12, pp. 2568-2576, Dec. 2005.
- [3] A. M. Ionescu and H. Riel, "Tunnel field-effect transistors as energy-efficient electronic switches," *Nature*, vol. 479, no. 7373, pp. 329-237, Nov. 2011.
- [4] M. T. Björk, J. Knoch, H. Schmid, H. Riel, and W. Riess, "Silicon nanowire tunneling field-effect transistors," *Appl. Phys. Lett.*, vol. 92, no. 19, pp. 193504-1-193504-3, May 2008.
- [5] A. Schenk, "Rigorous theory and simplified model of the band-to-band tunneling in silicon," *Solid State Electron.*, vol. 36, no. 1, pp. 19-34, Jan. 1993.
- [6] S. Mookerjee, D. Mohata, R. Krishnan, J. Singh, A. Vallett, A. Ali, T. Mayer, V. Narayanan, D. Schlom, A. Liu, and S. Datta, "Experimental demonstration of 100 nm channel length In_{0.53}Ga_{0.47}As-based vertical inter-band tunnel field effect transistors (TFET) for ultra low-power logic and SRAM applications," in *Proc. IEEE Int. Electron Devices Meeting*, 2009, pp. 1-3.
- [7] P. Zhao, J. Chauhan, and J. Guo, "Computational study of tunneling transistor based on graphene nanoribbon," *Nano Lett.*, vol. 9, no. 2, pp. 684-688, Feb. 2009.
- [8] Y. W. Son, M. L. Cohen, and S. G. Louie, "Energy gaps in graphene nanoribbons," *Phys. Rev. Lett.*, vol. 97, no. 21, pp. 216803-1-216803-4, Nov. 2006.
- [9] H. Raza and E. C. Kan, "Armchair graphene nanoribbons: Electronic structure and electric-field modulation," *Phys. Rev. B, Condens. Matter*, vol. 77, no. 24, pp. 245434-1-245434-5, Jun. 2008.
- [10] B. Radisavljevic, A. Radenovic, J. Brivio, V. Giacometti, and A. Kis, "Single-layer MoS₂ transistors," *Nat. Nanotechnol.*, vol. 6, no. 3, pp. 147-150, Mar. 2011.
- [11] B. Radisavljevic, M. B. Whitwick, and A. Kis, "Integrated circuits and logic operations based on single-layer MoS₂," *ACS Nano*, vol. 5, no. 12, pp. 9934-9938, Dec. 2011.
- [12] Y. Yoon, K. Ganapathi, and S. Salahuddin, "How good can monolayer MoS₂ transistors be?" *Nano Lett.*, vol. 11, no. 9, pp. 3768-73, Sep. 2011.
- [13] K. Mak, C. Lee, J. Hone, J. Shan, and T. Heinz, "Atomically thin MoS₂: A new direct-gap semiconductor," *Phys. Rev. Lett.*, vol. 105, no. 13, pp. 136805-1-136805-4, Sep. 2010.
- [14] A. Splendiani, L. Sun, Y. Zhang, T. Li, J. Kim, C.-Y. Chim, G. Galli, and F. Wang, "Emerging photoluminescence in monolayer MoS₂," *Nano Lett.*, vol. 10, no. 4, pp. 1271-1275, Apr. 2010.
- [15] Y. Li, Z. Zhou, S. Zhang, and Z. Chen, "MoS₂ nanoribbons: High stability and unusual electronic and magnetic properties," *J. Amer. Chem. Soc.*, vol. 130, no. 49, pp. 16739-16744, Dec. 2008.
- [16] C. Ataca, H. Sahin, E. Aktürk, and S. Ciraci, "Mechanical and electronic properties of MoS₂ nanoribbons and their defects," *J. Phys. Chem. C*, vol. 115, no. 10, pp. 3934-3941, Mar. 2011.
- [17] Q. Yue, S. Chang, J. Kang, X. Zhang, Z. Shao., S. Qin, and J. Li, "Bandgap tuning in armchair MoS₂ nanoribbon," *J. Phys.: Condens. Matter.*, vol. 24, no. 33, pp. 335501-1-335501-7, Aug. 2012.
- [18] *QuantumWise Simulator*, Atomistix ToolKit (ATK). [Online]. Available: <http://www.quantumwise.com/>
- [19] M. Luisier and G. Klimeck, "Simulation of nanowire tunneling transistors: From the Wentzel-Kramers-Brillouin approximation to full-band phonon-assisted tunneling," *J. Appl. Phys.*, vol. 107, no. 8, pp. 084507-1-084507-6, Apr. 2010.
- [20] R. K. Pandey, K. V. R. M. Murali, S. S. Furkay, P. J. Oldiges, and E. J. Nowak, "Crystallographic-orientation-dependent gate-induced drain leakage in nanoscale MOSFETs," *IEEE Trans. Electron Devices*, vol. 57, no. 9, pp. 2098-2105, Sep. 2010.
- [21] D. Kienle, J. I. Cerda, and A. W. Ghosh, "Extended Hückel theory for band structure, chemistry and transport. I. Carbon nanotubes," *J. Appl. Phys.*, vol. 100, no. 4, pp. 043714-1-043714-9, Aug. 2006.
- [22] J. Cerda and F. Soria, "Accurate and transferable extended Hückel-type tight-binding parameters," *Phys. Rev. B*, vol. 61, no. 12, pp. 7965-7971, Mar. 2000.
- [23] P. Pulay, "Convergence acceleration of iterative sequences the case of SCF iteration," *Chem. Phys. Lett.*, vol. 73, no. 2, pp. 393-398, Jul. 1980.
- [24] International Technology Roadmap for Semiconductors. [Online]. Available: http://www.itrs.net/Links/2009ITRS/2009Chapters_2009Tables/2009_ExecSum.pdf

- [25] Y. Sun, S. E. Thompson, and T. Nishida, *Strain Effect in Semiconductors: Theory and Device Applications*. New York: Springer-Verlag, 2010.
- [26] Z. H. Ni, T. Yu, Y. H. Lu, Y. Y. Wang, Y. P. Feng, and Z. X. Shen, "Uniaxial strain on graphene: Raman spectroscopy study and band-gap opening," *ACS Nano*, vol. 2, no. 11, pp. 2301–2305, Nov. 2008.
- [27] K. S. Kim, Y. Zhao, H. Jang, S. Y. Lee, J. M. Kim, K. S. Kim, J. H. Ahn, P. Kim, J. Y. Choi, and B. H. Hong, "Large-scale pattern growth of graphene films for stretchable transparent electrodes," *Nature*, vol. 457, no. 7230, pp. 706–710, Feb. 2009.
- [28] J. Kang, Y. He, J. Zhang, and X. Yu, "Modeling and simulation of uniaxial strain effects in armchair graphene nanoribbon tunneling field effect transistors," *Appl. Phys. Lett.*, vol. 96, no. 25, pp. 252105-1–252105-3, Jun. 2010.
- [29] X. Guan, D. Kim, K. C. Saraswat, and H.-S. P. Wong, "Complex band structures: From parabolic to elliptic approximation," *IEEE Electron Device Lett.*, vol. 32, no. 9, pp. 1296–1298, Sep. 2011.
- [30] S. M. Sze and K. K. Ng, *Physics of Semiconductor Devices*, 3rd ed. Hoboken, NJ: Wiley, 2007.
- [31] K. H. Kao, A. S. Verhulst, W. G. Vandenberghe, B. Soree, G. Groeseneken, and K. D. Meyer, "Direct and indirect band-to-band tunneling in germanium-based TFETs," *IEEE Trans. Electron Devices*, vol. 59, no. 2, pp. 292–301, Feb. 2012.
- [32] M. A. Khayer and R. K. Lake, "Drive currents and leakage currents in InSb and InAs nanowire and carbon nanotube band-to-band tunneling FETs," *IEEE Electron Device Lett.*, vol. 30, no. 12, pp. 1257–1259, Dec. 2009.
- [33] D. Jena, T. Fang, Q. Zhang, and H. Xing, "Zener tunneling in semiconducting nanotube and graphene nanoribbon p-n junctions," *Appl. Phys. Lett.*, vol. 93, no. 11, pp. 112106-1–112106-3, Sep. 2008.
- [34] Y. Ouyang, H. J. Dai, and J. Guo, "Projected performance advantage of multilayer graphene nanoribbons as a transistor channel material," *Nano Res.*, vol. 3, no. 1, pp. 8–15, Jan. 2010.



Ram Krishna Ghosh received the M.Sc. degree in physics from the Indian Institute of Technology Madras, Chennai, India, in 2008. He is currently working toward the Ph.D. degree at the Indian Institute of Science, Bangalore, India.



Santanu Mahapatra (M'08–SM'10) received the Ph.D. degree from the Ecole Polytechnique Federale de Lausanne, Lausanne, Switzerland, in 2005.

He is currently an Associate Professor with the Indian Institute of Science, Bangalore, India.